20th International Conference on Structural Mechanics in Reactor Technology (SMiRT 20)
Espoo, Finland, August 9-14, 2009
SMiRT 20-Division 8, Paper 2476

Fabrication Flaw Density and Distribution in Piping Weldments[1]

Steven R. Doctor

Pacific Northwest National Laboratory, Richland, Washington, USA, e-mail: steven.doctor@pnl.gov

Keywords: fabrication flaws, piping weldments, austenitic stainless steel, dissimilar metal welds.

1 ABSTRACT

The U.S. Nuclear Regulatory Commission supported the Pacific Northwest National Laboratory (PNNL) to develop empirical data on the density and distribution of fabrication flaws in nuclear reactor components. These data are needed to support probabilistic fracture mechanics calculations and studies on component structural integrity. PNNL performed nondestructive examination inspections and destructive testing on archived piping welds to determine the fabrication flaw size and distribution characteristics of the flaws in nuclear power plant piping weldments. Eight different processes and product forms in piping weldments were studied including wrought stainless steel and dissimilar metal weldments. Parametric analysis using an exponential fit was performed on the data. Results were created as a function of the through-wall size of the fabrication flaws as well as the length distribution. The results are compared and contrasted with those developed for reactor pressure vessel processes and product forms. The most significant findings were that the density of fabrication flaws versus through-wall size was higher in piping weldments than that for the reactor pressure vessel weldments, and the density of fabrication flaws versus through-wall size in both reactor pressure vessel weld repairs and piping weldments were greater than the density in the original weldments. Curves showing these distributions are presented.

2 INTRODUCTION

The U.S. Nuclear Regulatory Commission (NRC) initiated research activities in 1989 at the Pacific Northwest National Laboratory (PNNL) with the major objective of estimating the density of fabrication flaws in U.S. light water reactor pressure vessels (RPVs) and piping welds (Jackson et al. 2001). PNNL's methodology for estimating the density and size distribution of fabrication flaws involves the nondestructive evaluation (NDE) of weldments from cancelled nuclear plants and the destructive validation of detected flaws. This methodology characterizes the flaws for fracture mechanics significance because the likelihood of vessel failure is sensitive to flaw location, type, size, orientation, and other flaw characterizations (Simonen and Khaleel 1995). The objective of this research is to estimate these and other relevant properties of flaws created during the fabrication of nuclear component weldments.

To meet this objective, a generalized flaw distribution approach was used because the density of fabrication flaws is expected to vary over product forms and over the years of component fabrication. To develop a generalized flaw distribution and to resolve technical issues, an expert judgment process was used. The results of this expert judgment process helped to formulate a generalized approach to fabrication flaw density and distribution (Jackson and Abramson 2000). The impaneled experts concluded that the product forms and construction processes determine the fabrication flaws in weldments. So, for the *i*th component, the number of flaws greater than size *x* can be given by a sum over product forms.

$$N_i(x) = \sum_j \rho_j(t_i) \cdot V_{ij} \cdot G_j(x) \qquad (1)$$

[1] The work was sponsored by the U.S. Nuclear Regulatory Commission under U.S. Department of Energy Contract DE-AC05-76RL01830; NRC JCN Y6398; Mr. Wallace Norris, Program Monitor.

where $\rho_j(t_i)$ is the flaw density in product form *j* during time interval for the construction of the *i*th component t_i, V_{ij} is the volume (or area) of the product form in a weldment or a region of a weldment, and $G_j(x)$ is the probability that a flaw, in product form *j*, has a size greater than *x*. PNNL data have shown that

$$G_j(x) = \alpha \exp(-\beta_j x) \quad (2)$$

provides a reasonable fit to the fabrication flaw data (Doctor and Schuster 2001).

Estimates for flaw densities are an important input to structural assessments by fracture mechanics calculations. Component failure is an issue of increasing concern as the current operating nuclear power plants reach the middle to latter portion of their license periods and have accumulated service-related degradation. Computer codes require accurate estimates of the flaw densities in the reactor component to determine the likelihood of a component failure. The majority of past work in probabilistic fracture mechanics (PFM) considered cracks to be expressed in terms of a single crack size parameter (size in the depth dimension). A two-dimensional crack is much more realistic but considerably more complex. Some PFM codes are capable of treating two-dimensional cracks and are based on the assumption that a two-dimensional crack is a semi-elliptical surface crack.

This paper describes the work PNNL performed involving NDE inspections and destructive analysis on archived piping weldments to determine the fabrication flaw size and distribution characteristics. Available materials were collected and prioritized for inclusion in this study, and the study focused on wrought-to-wrought stainless steel and dissimilar metal welds.

3 TECHNICAL APPROACH

Collection of scientific data began with the measurement of responses from machined reflectors installed in representative weld metal. The purpose of measuring these responses was to prove penetration by ultrasound into and possibly through the weld metal. In this way, the measurement procedure, ultrasonic frequency, and insonification angles were established for obtaining estimates of fabrication flaw density and distribution. Two evaluations of ultrasonic penetration through the base metal and the weld metal were made—one using inspections from the inside or outside surface, and one using a machined surface parallel to the weld for what PNNL calls a weld-normal insonification. At first, hole standards were configured for inspection from the inside or outside surface. After it was established that the responses from side-drilled holes (SDHs) could be reliably detected from the inside or outside surface, the hole standards were prepared for weld-normal testing. Figure 1 shows the wrought austenitic stainless steel to wrought austenitic stainless steel weld #6 with a specimen removed for use as a hole-standard.

Figure 2 shows side 1 of the wrought-to-wrought hole-standard with three of five SDHs. The holes are 1.5 mm in diameter. SDH #1 is in the middle of the weld's root pass—a tungsten gas arc weld. SDH #2 is in the middle of the shielded metal arc weld (SMAW) passes. SDH #3 is near the fusion zone of the SMAW with the stainless steel. Hole #3 has 2 mm of weld metal between it and the stainless steel base metal.

Figure 3 shows side 2 of the wrought-to-wrought hole-standard with two of five SDHs. SDH #4A is on the weld center line in the shielded metal arc weld. SDH #4B is in the fusion zone of the SMAW with the stainless steel.

Table 1 gives the 45° shear detection results from the wrought-to-wrought hole-standard. The table shows the results from 10-MHz, 45° shear waves applied from the inside of the pipe (the scanning was performed on the pipe's inside surface). The modality detected the notch using a full Vee path (reflection from the outside surface of the pipe). The modality detected hole #1 from both directions. Holes #4A and #4B were detected from only one direction. The other holes were not detected by the 45° shear waves.

In a similar manner, other frequencies, inspections angles, and modalities were systematically assessed to determine the most effective combinations for each of the materials in the specimens examined in this study. Ultimately, the weld-normal inspection modality was found to provide the best performance coupled with data processing using the synthetic aperture focusing technique (SAFT). Figure 4 contains SAFT-UT images of a 1.5-mm diameter SDH in the wrought-to-wrought weld hole-standard. The location of SDH #3 is

shown in Fig. 2. The image shows that the 10-MHz compression (L) wave detected the hole from the near side—through the 2 mm of weld metal.

Figure 1. Weld #6 with calibration specimen removed from weld

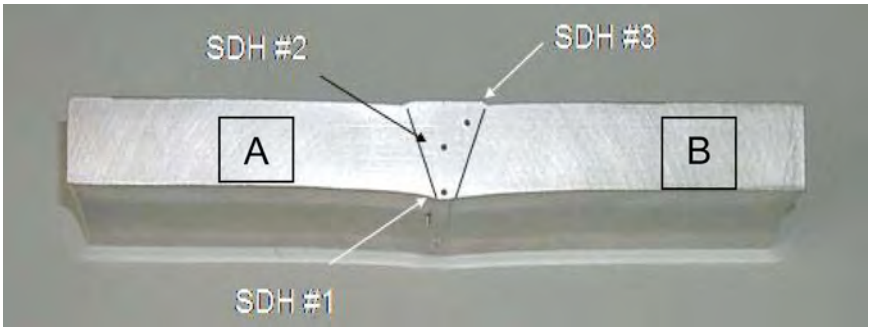

Figure 2. Wrought-to-wrought stainless steel (SS) calibration standard showing three of five side-drilled holes. Fusion lines of the weld with the base metal have been drawn in to add clarity to the location of the SDHs.

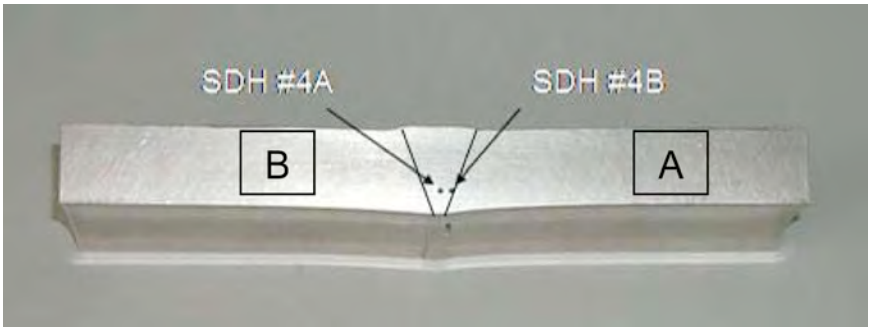

Figure 3. Wrought-to-wrought SS calibration standard showing two of five side drilled holes. Fusion lines of the weld with the base metal have been drawn in to add clarity to the location of the SDHs.

Table 1. Detection results for wrought-to-wrought stainless steel weld

10-MHz, 45° Shear		
	Side A	**Side B**
SDH #3	No	No
SDH #4B	Yes	No
SDH #1	Yes	Yes
SDH #2	No	No
SDH #4A	No	Yes

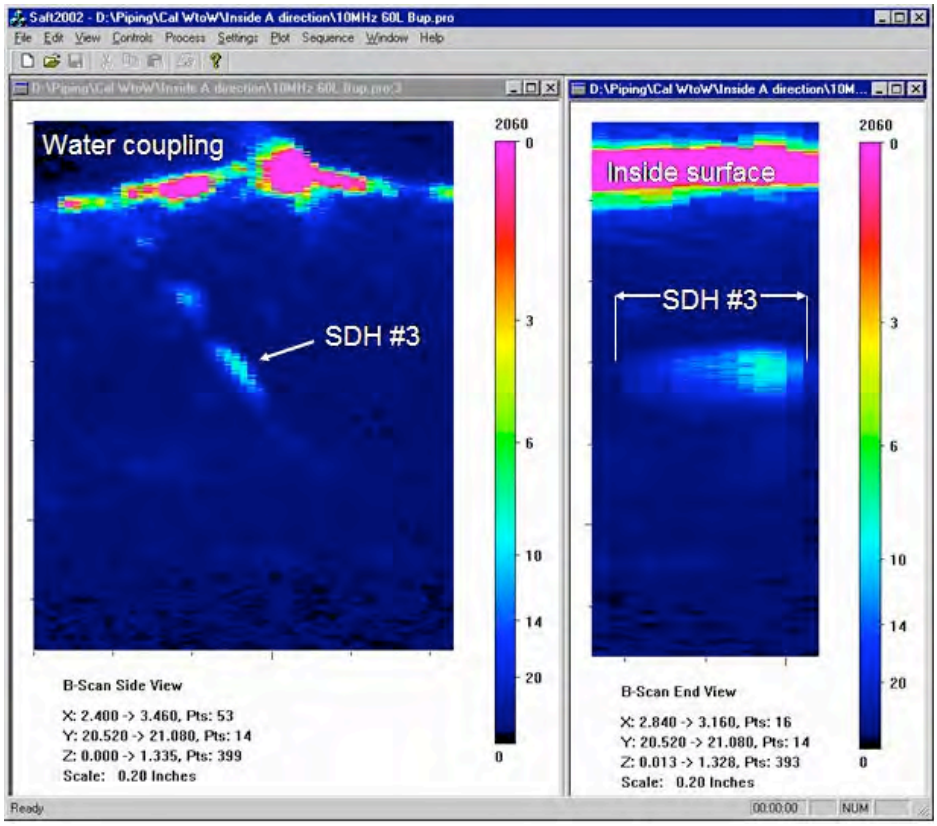

Figure 4. SAFT-UT images of 1.5-mm-diameter SDH in wrought-to-wrought SS weld calibration specimen

Figure 5 shows the piping weldments after they have been cut into rings for use in weld-normal inspections for this study.

Figure 5. Weld specimens employed in this study

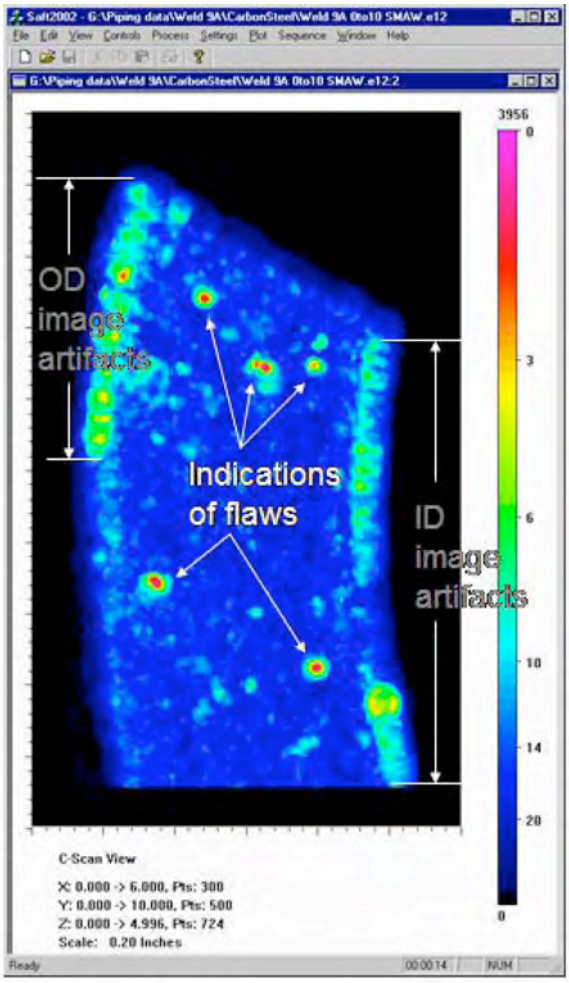

Figure 6. Top (C-scan) view image of the segmented ultrasonic responses from SMAW of a DMW

Figure 6 shows a typical weld-normal SAFT inspection result with some of the indications highlighted as well as some image artifacts. Figure 7 shows the results of a piping location where both an outside surface and an inside surface repair has been made.

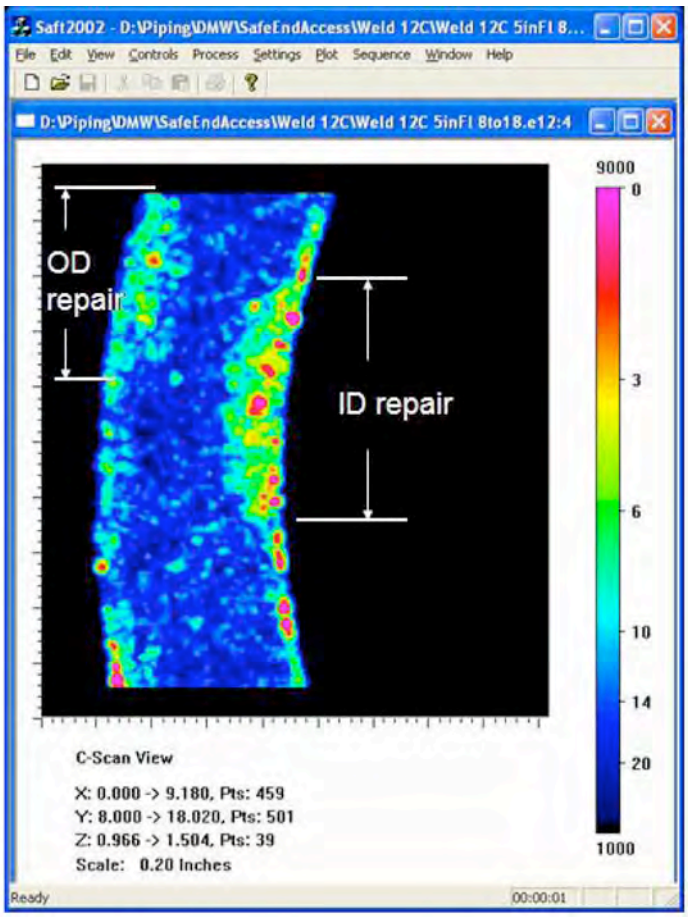

Figure 7. Top (C-scan) view image of the segmented ultrasonic responses from the safe end of a dissimilar metal weld showing two repairs (crescent-shaped areas) to the fusion zone of the SMAW with the safe end

4 WROUGHT AUSTENITIC STAINLESS STEEL PIPE WELDS

Two wrought austenitic stainless steel pipe welds were inspected with weld-normal testing: Beaver Valley pipe-to-pipe welds #6 and weld #7. Beaver Valley pipe-to-pipe weld # 6 is made of wrought austenitic stainless steel Type 316. The pipe outside diameter is 22 cm and thickness is 2.3 cm. The weld type is gas tungsten arc (GTAW) for the root pass and SMAW for the fill passes. The width of the weld crown is 2.3 cm. The fusion zone area is 310 cm^2 and weld volume is 190 cm^3.

For Beaver Valley pipe-to-pipe weld # 7, the pipe is made of wrought austenitic stainless steel Type 304. The pipe outside diameter is 22 cm and thickness is 1.3 cm. The weld type is GTAW for the root pass and SMAW for the fill passes. The width of the weld crown is 2.0 cm. The fusion zone area is 200 cm^2 and weld volume is 120 cm^3.

All of the material in welds #6 and #7 was inspected and analyzed. Table 2 lists the dimensions of the two wrought austenitic stainless steel welds. Table 3 shows the weld volumes and fusion zone areas.

Table 2. Dimensions of wrought-to-wrought weld specimen

	Pipe Thickness, cm	Weld Cross Section, cm	Weld Length, cm
Weld #6	2.3	3.0	62
Weld #7	1.3	1.9	64

Table 3. Inspected areas and volumes in wrought-to-wrought weld specimens

	Fusion Zone Area, cm^2	Weld Volume, cm^3
Weld #6	310	190
Weld #7	200	120
Total	510	310

Using the weld-normal ultrasonic inspections, nine flaw indications were found in the fusion zone of the SMAW with the wrought austenitic pipe. Table 4 gives the flaw frequency distributed in four through-wall sizes. In the validation testing, the nine flaw indications were extracted into 25-mm cubes. Table 5 lists the ultrasonic inspection results from the validation cubes.

Flaw frequency data in Tables 4 and 5 are used to calculate the cumulative flaw indication frequency and then the cumulative flaw frequency is normalized to the area of the weld fusion zone using the amount of material in the weld specimens as given in Table 3. Table 4 gives the density and unvalidated through-wall dimension distribution for the nine flaw indications found in the fusion area of the SMAW with the pipe's base metal. Table 5 gives the validated density as a function of cumulative through-wall dimension.

Table 4. Unvalidated through-wall size distribution for flaws in wrought-to-wrought SS weld specimens #6 and #7

Through-Wall Dimension	1.6 mm	2.1 mm	2.6 mm	3.1 mm
Frequency	1	5	1	2
Cumulative Frequency	9	8	3	2
Density, cm^{-2}	0.018	0.016	0.006	0.004

Table 5. Validated through-wall size distribution for flaws in wrought-to-wrought SS weld specimens #6 and #7

Through-Wall Dimension	1.3 mm	1.5 mm	1.8 mm
Frequency	3	3	2
Cumulative Frequency	8	5	2
Density, cm^{-2}	0.016	0.010	0.004

The flaw indication cumulative density and distribution data are charted with exponentially decreasing functions that are fit to the empirical data. The cumulative density and distribution function is

$$C(x) = \alpha e^{-\beta x}. \quad (3)$$

Figure 8 shows the flaw density and through-wall size distributions with their exponential fits. The validated estimate of flaw density in the fusion zone is 0.55 flaws per square cm. The slope parameter for the exponential fit to through-wall sizes is 2.7 per mm. The length of the flaws in the validation cubes was the same as their through-wall dimension.

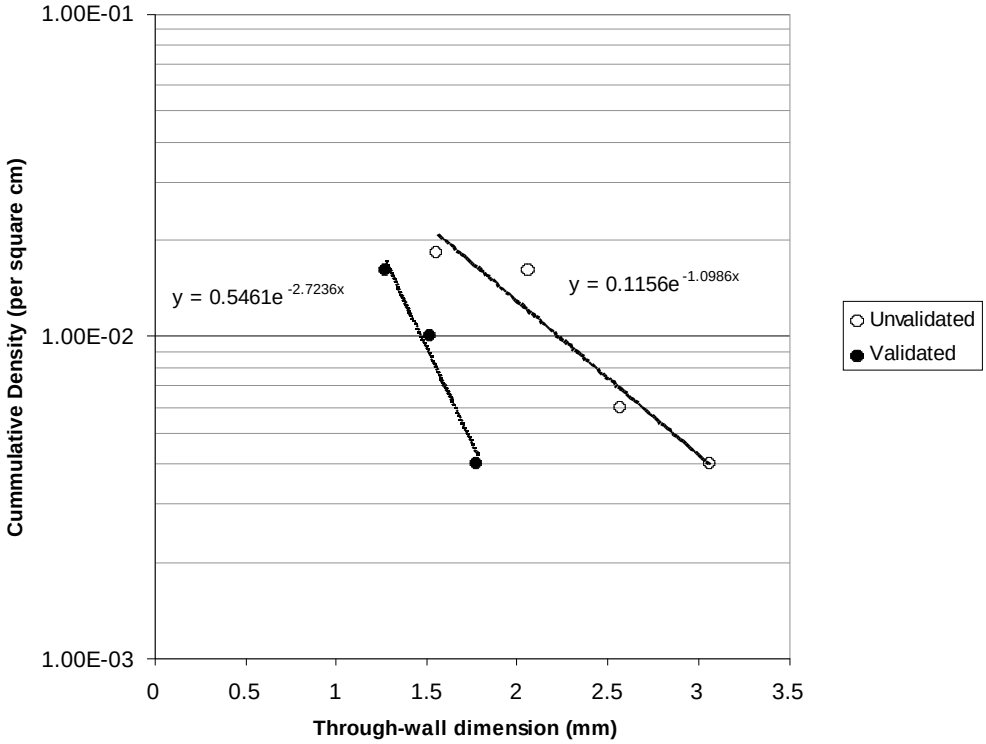

Figure 8. Cumulative through-wall size distribution for flaws in wrought-to-wrought SS weld specimen #6 and #7

5 DISSIMILAR METAL WELDS

Four dissimilar metal welds were inspected with weld-normal testing: cold leg safe-end to elbow bi-metallic weld #9, cold leg safe-end to pipe bi-metallic welds #12 and #20, and cold leg safe-end to nozzle bi-metallic weld #21.

For cold leg safe-end to elbow bi-metallic weld #9, the elbow is carbon steel (A516) with cladding (304L) and the safe-end is stainless steel (316). The diameter is 91 cm and thickness is 8.9 cm. Weld metal is 182 Inconel for buttering and for fill passes. The weld geometry has a 7.5° bevel and the crown width is 5.1 cm.

For cold leg safe-end to pipe bi-metallic welds #12 and #20, the pipe is carbon steel (A516) with cladding (304L) and the safe-end is stainless steel (316). The diameter is 91 cm and thickness is 8.9 cm. Weld metal is 182 Inconel for buttering and for fill passes. The weld geometry has a 7.5° bevel and the crown width is 5.1 cm.

For cold leg safe-end to nozzle bi-metallic weld #21, the nozzle is carbon steel (A516) with cladding (304L) and the safe-end is stainless steel (316). The diameter is 33 cm and thickness is 3.8 cm. Weld metal is 182 Inconel for buttering and for fill passes. The weld geometry has a 7.5° bevel and the crown width is 5.1 cm.

In the case of dissimilar metal welds, there are a number of interfaces that were independently evaluated to assess the flaw occurrence at each of these. There is the buttering to carbon steel fusion zone, the buttering inter-run flaws, the buttering to SMAW fusion zone, and the SMAW to safe-end fusion zone. The process that was employed is identical to that already described for the wrought-to-wrought case. In this paper, it is simply not possible to provide all of the study details; thus, only the most significant results will be shown in the next section.

6 DISCUSSION AND SUMMARY

An estimate of flaw density and distribution has been made for eight process and product forms in piping weldments. Parametric analysis using an exponential fit was performed. The results for through-wall size are

given in Table 6. The results of a parametric fit for the length distribution are given in Table 7. For comparison, the flaw density and distribution in RPV's machine-made weld passes can be found in Table 8.

Table 6. Exponential fit results for through-wall dimension

	α	
SS to SS	0.55 cm^{-2}	2.7 mm^{-1}
Buttering to Carbon Steel	0.14 cm^{-2}	0.94 mm^{-1}
Buttering Inter-Run	0.10 cm^{-3}	1.3 mm^{-1}
Buttering to SMAW	0.75 cm^{-2}	1.1 mm^{-1}
SMAW to Safe-End	1.2 cm^{-2}	1.6 mm^{-1}
Repairs	0.37 cm^{-2}	0.81 mm^{-1}
SMAW to SCSS Elbow	0.15 cm^{-2}	0.78 mm^{-1}
SMAW to CCSS Pipe	0.097 cm^{-2}	0.55 mm^{-1}

Table 7. Exponential fit results for length distribution

	α	
SS to SS	0.55 cm^{-2}	2.7 mm^{-1}
Buttering to Carbon Steel	0.13 cm^{-2}	0.60 mm^{-1}
Buttering Inter-Run	0.16 cm^{-3}	0.98 mm^{-1}
Buttering to SMAW	0.11 cm^{-2}	0.41 mm^{-1}
SMAW to Safe-End	0.44 cm^{-2}	0.52 mm^{-1}
Repairs	0.37 cm^{-2}	0.81 mm^{-1}
SMAW to SCSS Elbow	0.51 cm^{-2}	0.84 mm^{-1}
SMAW to CCSS Pipe	1.2 cm^{-2}	0.56 mm^{-1}

Table 8. Reactor pressure vessel flaw distribution parameters for various product forms

	α	
SAW, PVRUF RPV	0.013 cm^{-2}	1.2 mm^{-1}
SAW, Shoreham RPV	0.050 cm^{-2}	1.2 mm^{-1}
RPV Repairs	0.13 cm^{-2}	0.18 mm^{-1}

Figure 9 shows a comparison of flaw density and through-wall size distributions from the piping and the RPV research. All densities are given in flaws per square centimeter. RPV repairs were found to have large flaws on the ends of the repair cavities, but this was not found to be the case for the repairs to dissimilar

metal welds. The submerged arc weld (SAW) in the PVRUF vessel had the lowest flaw rate of the material examined to date. The flaw rates for the piping weldments typically fall above the Shoreham SAW's flaw rate.

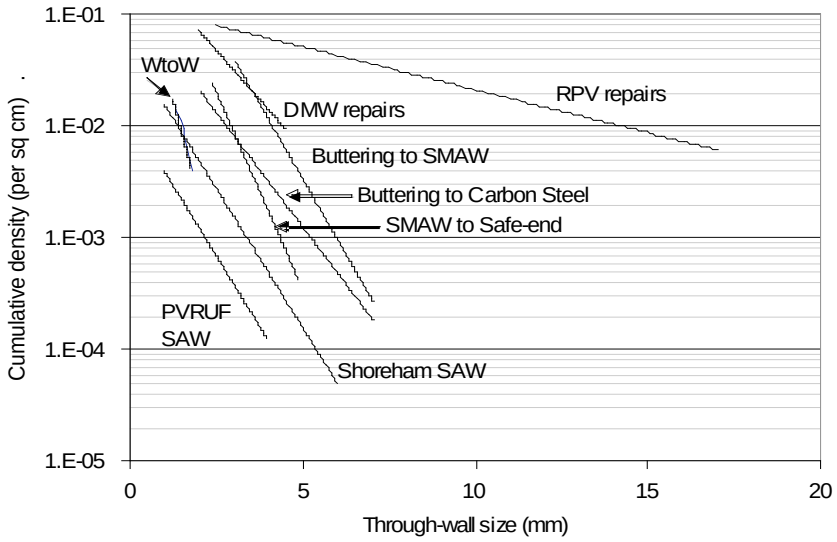

Figure 9. Comparison of flaw density and through-wall size distributions. (Note: Wrought-to-wrought is the same as SS to SS).

Additional work that is done to improve the estimates of flaw density and distribution in piping welds should include testing of thicker wrought-to-wrought welds, acquisition of additional weld repairs, and studies on flaws in cast stainless steel weldments. The wrought-to-wrought welds #6 and #7 were 23-mm and 12-mm thick. Wrought austenitic stainless steel pipe to elbow welds that are 75-mm thick should be tested for fabrication flaw density and size distribution.

In summary, only a limited amount of material in each product form was studied. It would be useful to expand this study to additional weldments in order to obtain better density and distribution statistics and determine if the trends stay the same or change.

Acknowledgments

The author thanks George J. Schuster for his efforts and outstanding contributions. Mr. Schuster, who is now retired, was the key PNNL staff person that oversaw the conduct of the work reported in this paper.

REFERENCES

Doctor, S. R. and Schuster, G. J. 2001. Destructive Validation Methodology and Results for the Characterization of Flaws in Nuclear Reactor Pressure Vessels. In 3rd International Conference of NDE in Relation to Structural Integrity for Nuclear and Pressurized Components. Seville, Spain, November 14-16, 2001.

Jackson, D. A. and Abramson, L. 2000. Report on the Preliminary Results of the Expert Judgment Process for the Development of a Methodology for a Generalized Flaw Size and Distribution for Domestic Reactor Pressure Vessels. Washington, D.C.: U.S. Nuclear Regulatory Commission. MEB-00-01, PRAB-00-01.

Jackson, D. A., Doctor, S. R., Schuster, G. J. and Simonen, F. A. 2001. Developing a Generalized Flaw Distribution for Reactor Pressure Vessels. Nuclear Engineering and Design. Vol. 208. P 123-131.

Simonen, F. A. and Khaleel, M. A. 1995. A Model for Predicting Vessel Failure Probabilities Due to Fatigue Crack Growth. In Pressure Vessel and Piping Conference. Fatigue and Fracture Mechanics, PVP Vol. 304. American Society of Mechanical Engineers, New York. P. 401-416.